Development of low-profile piezoelectric energy harvester for high load application

Thorin Purviance, Spencer Wickler, Keith Clayson, Travis Barnes, and Changki Mo
School of Mechanical and Materials Engineering
Washington State University Tri-Cities
Richland, U.S.A.
changki.mo@tricity.wsu.edu

***Abstract*—This paper examines the feasibility of a low-profile piezoelectric energy harvester that is particularly useful in application where it is used as power source from high mechanical load and imbedding it in the limited space. Two low-profile energy harvesting devices - a piezoelectric ring transducer and set of PZT stacks are designed and tested. The first proposed energy harvester is composed of a ring transducer, metal outer ring, and cymbal metal end caps. The top and bottom cymbal metal end caps are placed inside the ring and transfer the applied mechanical load on the apex to the inner circumference of the piezoelectric ring transducer by compressing it. The new design is beneficial because applied load gives rise to compressive stress in the piezoelectric layer. A second design is introduced using an array of piezoelectric stacks arranged around cymbal shaped springs. By using compressive stress to the PZT, energy generating performance of the proposed design can be significantly improved comparing to the previous cymbal design using either PZT mono-layer or unimorph PZT. In addition, for the new design high shear strength of the bonding layer is not required to resist amplified radial stress through metal end caps comparing to the previous design.**

Keywords—Energy harvesting; cymbal-structured; low-profile; piezoelectric; ring and stack transducers; compressive stress.

I. INTRODUCTION

Energy Harvesting has been a subject of major research over the past decade for its use as a self-sustaining energy source. There is demand for self-sustainable energy devices in a variety of applications including wearable electronics, wireless sensor nodes, biomedical systems, etc. This paper explores the design, fabrication, and testing for power generation of a low-profile cymbal piezoelectric energy harvesting device. The cymbal-structured energy harvester is a small autonomous device that uses lead zirconate titanate (PZT) to generate electrical energy, utilizing very low excitation frequency of 1Hz, under high load, and in a confined space. Unimorph [1-3] and bimorph [4] cymbal piezoelectric energy harvesters were developed, fabricated and tested [1-3] for higher load application comparing to the harvester of mono-layered cymbal structure [5-8]. It was demonstrated that the unimorph cymbal harvester generated useful energy while withstanding much higher load of about 2,000 N. Fig. 1 shows previously explored designs of the cymbal energy harvester. The cymbal was used to transform mechanical load into a tensile force on the PZT/steel composite between metal end caps, however, it was found that the tension yield strength of the material was a limiting factor. The arrows in Fig. 1 represent the radial tensile stress due to compressive load applied to the metal end caps.

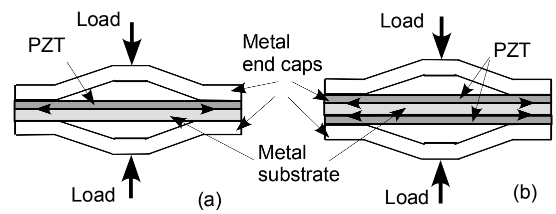

Figure 1: Comparison of Previously Explored PZT Cymbal Structures: (a) Unimorph [1-3] and (b) Bimorph [4].

Noting that the compressive yield stress of piezoelectric material is much higher than the tensile yield strength, two cymbal piezoelectric energy harvesting devices were constructed which utilize compressive stress in the PZT structure, rather than tensile, to produce more energy. The piezoelectric material has a tensile yield stress of approximately 35MPa; while in compression the yield stress was estimated by the manufacturer to be 270MPa (STEINER & MARTINS, Inc).

In order to alleviate the tensile overload issues associated with the previous cymbal structure devices, the cymbal was restructured with a piezoelectric ring (SM411, STEINER & MARTINS, Inc) sandwiched concentrically between a cymbal based load transformer and a retaining ring. This was done in order to achieve a higher compressive load on the PZT material. The cymbal-structured metal end caps will compress the PZT material by expanding radially outward against the inner wall of the PZT ring. The tensile stresses are still the limiting factor, however the tensile stresses in this design will be incidentally induced hoop stresses in the material rather than directly applied tension. In order to maximize the power output of the piezoelectric device, this design will increase the stress in the material as close as possible to the compressive yield strength of the material.

The piezoelectric ring was found to be poled in axial direction (d_{31} mode) not radial direction (d_{33} mode). The ring transducer was replaced by four set of compact size PZT stack transducer (SMPAK15553D4, STEINER & MARTINS, Inc). This restructured cymbal design is advantageous to the limited space application comparing to the regular piezoelectric stack harvesters [9-11].

With those advantages the alternative cymbal design could be applied to orthopedic implants such as total knee replacement (TKR) [9-11] where imbedding space is typically confined but power is required to operate embedded sensors monitoring the state of implants [12, 13]. This cymbal harvester could be also explored as a low-profile power generator for floors and roadways.

Analytical modeling to predict the performance of the new cymbal design is carried out. A test rig was built, which consists of NI LabVIEW, Arduino-based data acquisition and control system for the test. The cymbal specimens were fabricated and test results under cyclic loads of 800 N, 1500 N, and 2,100 N are presented. It was assumed that loads of about 2-3 times that of standard human body weight would be imposed on the cymbal in the normal walking condition [1-4, 14].

II. Design & Analysis

The design of the piezoelectric energy harvesting devices consists of three main components: the outer retaining ring, the piezoelectric material oriented for compressive stresses, and the cymbal in the center.

A. *First Iteration*

This iteration utilized a piezoelectric ring transducer to transform the mechanical energy imparted from the cymbal. This was chosen in order to maximize the occupation of space between the cymbal and outer ring, and minimize inadvertent lateral and tensile stresses imposed in the PZT structure as shown in Fig. 2 and Fig. 3.

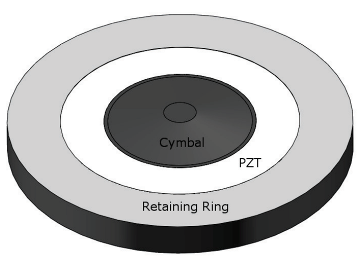

Figure 2: Schematic of First Iteration Design.

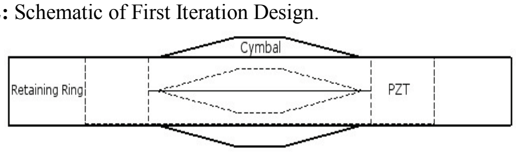

Figure 3: Schematic of First Iteration Cross Section.

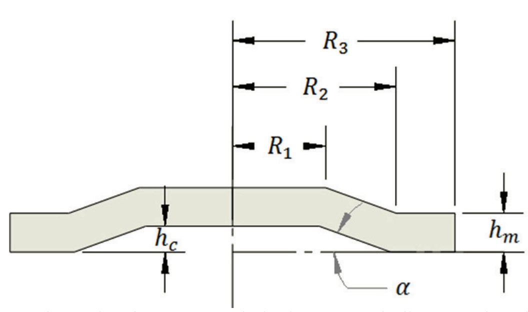

Figure 4: Schematic of Upper Cymbal Diagram Including Metal End Cap and Cavity Height.

In the schematic for the cross section of the cymbal as depicted in Fig. 4, R_1 is the radius of the apex, R_2 is the radius of the cavity, R_3 is the radius of the end cap, h_m is the material thickness, h_c is the cavity height, and α is the angle to form the end cap cavity.

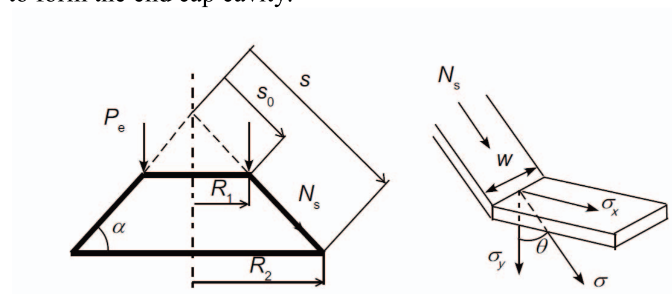

Figure 5 : Configuration of a Truncated Conical Shell for Analysis [2, 3].

The cymbal can be viewed as a truncated conical shell as shown in Fig. 5 [2, 3]. When a load is applied to the radius of the apex, R_1; the in-plane force per unit circumference N_s can be determined by [15].

$$N_s = -\frac{s_0}{s} P_e \frac{1}{\sin(\alpha)} \tag{1}$$

Where s is the radial distance from the imaginary apex of the cone to the outer edge and s_0 is the distance from the apex to the top of the cavity. Where the angle forming the end cap cavity is described as: $\alpha = \tan^{-1}\left(\frac{h_c}{R_2 - R_1}\right)$. The stress is described as $\sigma = \frac{N_s}{h_m w}$ which can be decomposed into the stress in the radial direction $\sigma_x = \sigma \sin(\theta)$. Where w is per unit width and $\theta = \frac{\pi}{2} - \alpha$.

When everything is combined the equation for the stress in the radial direction simplifies to $\sigma_x = -\frac{s_0}{s} P_e \frac{\sin(\theta)}{\sin(\alpha) h_m w}$.

It is assumed that the stress applied by the cymbal is applied uniformly over the interior of the cylindrical PZT shell $q = \sigma_x$ (Fig. 6). The stress in a thick walled cylindrical disk or shell with uniform internal radial pressure q, longitudinally pressure zero or externally balanced, for a disk or a shell can be described as $\sigma_3 = -\frac{qb^2(a^2 - r^2)}{r^2(a^2 - b^2)}$. Where a is the outer radius of the PZT shell, b is the inner radius.

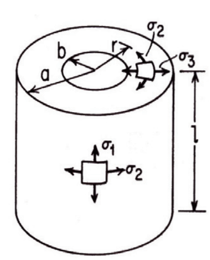

Figure 6: Cylindrical Shell [16].

Combining everything yields a radial stress equation of $\sigma_3 = \frac{-\sigma_x b^2(a^2 - r^2)}{r^2(a^2 - b^2)}$.

To determine the power generated by the transducer, the energy of a small volume of material is modeled as, $dU_c = \frac{1}{2} e_c \sigma_3 + \frac{1}{2} D_{3c} E_3$. Where e_c is the compressive strain in the piezoelectric material. D_{3c} is the charge density of the material due to compressive stresses.
The constitutive equations [17] can be written as

$$e_c = S_{11}^E \sigma_3 - d_{31} E_3 \text{ , } D_{3c} = -d_{31} \sigma_3 + \epsilon_{33}^T E_3 \tag{2}$$

Where d_{31} is a piezoelectric constant, S_{11}^E is the piezoelectric material eleastic compliances and ϵ_{33}^T is the permittivity of the piezoelectric material.
Substitute the electric field E_3 with $\frac{V}{l}$ where l is the height of the PZT material. Then integrate over the entire structure:

$$U = \int_b^a \int_0^{2\pi} \left(\int_0^l dU_c \, dz \right) r \, d\theta \, dr \tag{3}$$

which becomes

$$U = \frac{\pi V^2 \epsilon_{33}^T}{2l} (a^2 - b^2) + \frac{\pi \, P_e \, V \, d_{31} \, s_0 \, \sin(\theta)}{h_m \, s \, w \, \sin(\alpha)(a^2 - b^2)} (a^2 \, b^2 - b^4) + \frac{\pi P_e^2 S_{11} l s_0^2 \sin(\theta)^2}{2 h_m^2 \, s^2 \, w^2 \, \sin(\alpha)^2 \, (a^2 - b^2)^2} (a^2 b^4 - b^6) - \frac{2 \, \pi \, P_e \, V \, a^2 \, b^2 \, d_{31} \, s_0 \, \sin(\theta)(\ln(a) - \ln(b))}{h_m \, s \, w \, \sin(\alpha) \, (a^2 - b^2)} - \frac{\pi \, P_e^2 \, S_{11} \, a^2 \, b^4 \, l \, s_0^2 \, \sin(\theta)^2}{h_m^2 \, s^2 \, w^2 \, \sin(\alpha)^2 \, (a^2 - b^2)^2} \left\{ a^2 \left(\frac{1}{2 * a^2} - \frac{1}{2 * b^2} \right) - 2(\ln(a) - \ln(b)) \right\} \tag{4}$$

Differentiate U to find the charge

$$Q = \frac{\pi \, V \, \epsilon_{33}^T}{l} (a^2 - b^2) + \frac{\pi \, P_e \, d_{31} \, s_0 \, \sin(\theta)}{h_m \, s \, w \, \sin(\alpha) \, (a^2 - b^2)} (a^2 b^2 - b^4) - \frac{2 \, \pi \, P_e \, a^2 \, b^2 \, d_{31} \, s_0 \, \sin(\theta) \, (\ln(a) - \ln(b))}{h_m \, s \, w \, \sin(\alpha) \, (a^2 - b^2)} \tag{5}$$

If there is no applied external electric field then (*V*= 0). Which gives us the charge generated Q_{gen}.

$$Q_{gen} = \frac{\pi \, P_e \, d_{31} \, s_0 \, \sin(\theta)}{h_m \, s \, w \, \sin(\alpha) \, (a^2 - b^2)} (a^2 b^2 - b^4) - \frac{2 \, \pi \, P_e \, a^2 \, b^2 \, d_{31} \, s_0 \, \sin(\theta) \, (\ln(a) - \ln(b))}{h_m \, s \, w \, \sin(\alpha) \, (a^2 - b^2)} \tag{6}$$

Utilizing the *Q*= *CV* relationship, open circuit capacitance, C_{free} is:

$$C_{free} = \frac{\pi \, \epsilon_{33}^T}{l} (a^2 - b^2) \tag{7}$$

$$V_{gen} = \frac{Q_{gen}}{C_{free}} \tag{8}$$

$$U_{gen} = \frac{1}{2} C_{free} V_{gen}^2 f \tag{9}$$

B. Second Iteration

The second design was utilized to take advantage of commercially available stacked PZT structures (Figs. 7 and 8) capable of developing relatively more power than the single layer.

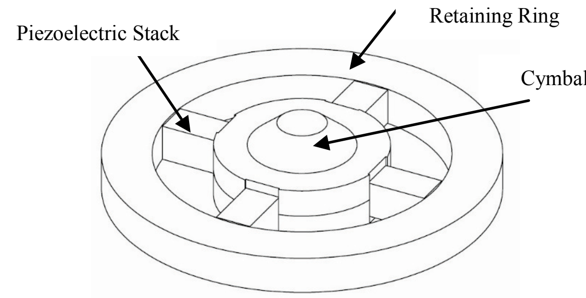

Figure 7: Schematic of Second Iteration Design.

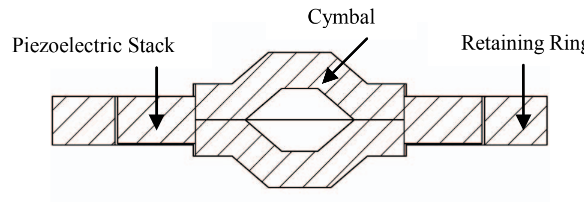

Figure 8: Schematic of Second Iteration Cross Section.

The same procedure from the first iteration is used. The stress in the radial direction is the same equation as above the only difference is the value of the width that the stress is applied over. Using the same constitutive equations we integrate over the entire structure $U = \int_0^d \int_0^w \left(\int_0^{2h_m} dU_c \, dz \right) \, dx \, dy$. Where *d* is the depth of the piezoelectric material, *w* is the combined total of the piezoelectric material stacks and h_m is the height of the piezoelectric material that is excited by one cymbal.

$$U_{total} = \frac{V^2 d \, \epsilon_{33} \, w}{4 \, h_m} + \frac{V \, C_1}{h_m \, C_2} + \frac{V \, C_1 \, (R_1 - R_2)^2}{h_c^2 \, h_m \, C_2} + \frac{P_e^2 \, R_1^2 \, S_{33} \, d \sin\left(\frac{\pi}{2} + \operatorname{atan}\left(\frac{h_c}{R_1 - R_2}\right)\right)^2 * \left(\frac{h_c^2}{(R_1 - R_2)^2} + 1\right)^2 (R_1 - R_2)^4}{h_c^4 \, h_m \, w \, (C_2)^2} \tag{10}$$

Where C_1 and C_2 defined as

$$C_1 = P_e \, R_1 \, d \, d_{33} \, \sin\left(\frac{\pi}{2} + \operatorname{atan}\left(\frac{h_c}{R_1 - R_2}\right)\right) \tag{11}$$

$$C_2 = \sqrt{(R_1 - R_2)^2 + h_c^2} - \frac{R_1 \sqrt{\frac{h_c^2}{(R_1 - R_2)^2} + 1 \, (R_1 - R_2)}}{h_c} \tag{12}$$

Differentiate U_{total} to find the charge

$$Q = \frac{V \, d \, \epsilon_{33} \, w}{2 \, h_m} + \left[\frac{C_1}{C_2}\right] \left\{ \frac{1}{h_m} + \frac{(R_1 - R_2)^2}{h_c^2 \, h_m} \right\} \tag{13}$$

If there is no applied external electrical field then the voltage is zero which yields the voltage generated.

$$Q_{gen} = \left[\frac{C_1}{C_2}\right] \left\{ \frac{1}{h_m} + \frac{(R_1 - R_2)^2}{h_c^2 \, h_m} \right\} \tag{14}$$

Using the *Q*= *CV* relationship we can determine

$$C_{free} = \frac{d \, \epsilon_{33} \, w}{2 \, h_m} \tag{15}$$

$$V_{gen} = \frac{Q_{gen}}{C_{free}} \tag{16}$$

$$U_{gen} = \frac{1}{2} C_{free} V_{gen}^2 \tag{17}$$

III. FABRICATION & EXPERIMENT

A. Fabrication of Test Specimens

The cymbals were fabricated from circular metal discs cut out by a water jet. The discs were cut out from a sheet of 2.3 mm thick 4140 alloy steel. The specifications for the disc fabrication are shown in Fig. 9.

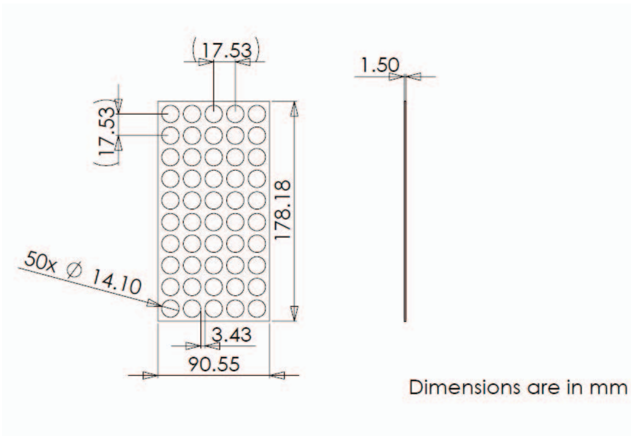

Figure 9: Cymbal Water Jet Cutout.

Each disk was compressed between the die and punch at 111.2 kN (25,000 lbs) in the Tinus Olsen testing machine. The cymbals were then epoxied into the harvesting devise and test leads where attached to the PZT material using conductive silver epoxy (CW2400, CircuitWorks). A finished energy harvester is shown in Fig. 10.

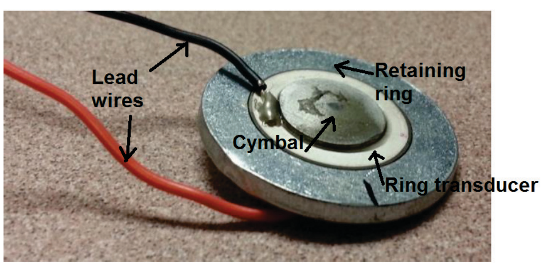

Figure 10: Photograph of the Finished PZT Cymbal Energy Harvester.

For the second design concept (Fig. 11), a washer will be fabricated into a retaining ring similar to the initial design. The same metal discs will be used to create the cymbals for this design iteration. A new punch and die will be created, heat treated and used to create the cymbals. Each of the parts will receive some epoxy that will lock the components in place.

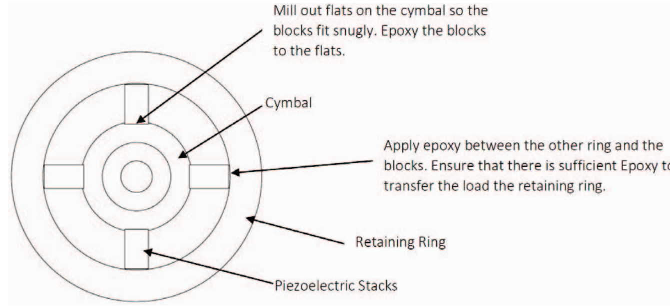

Figure 11: Second Iteration Fabrication Design.

Fabricated specimen is shown in Fig. 12. The electrical wires are also attached using the epoxy.

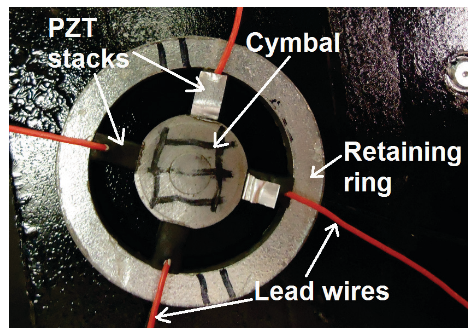

Figure 12: Photograph of the Fabricated Cymbal.

The cymbal specimen was tested on the test apparatus built for this project using cyclic loads of 800 N, 1,500 N, and 2,100 N at a frequency of 1 Hz. Fig. 13 shows an overview of the test rig used to test the cymbal specimen. A closed-up cymbal specimen in the test rig is shown in Fig. 14.

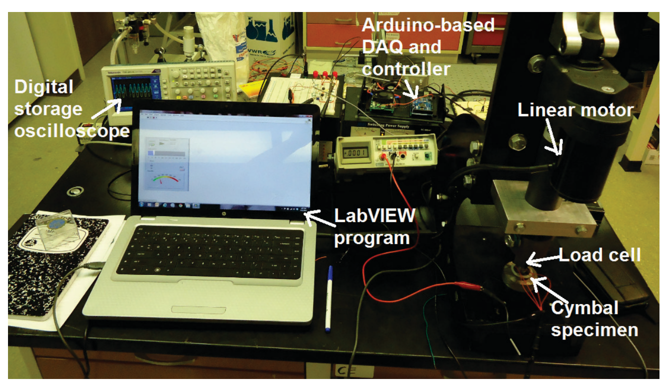

Figure 13: Photograph of the Test Rig Used to Test the Cymbal Specimen.

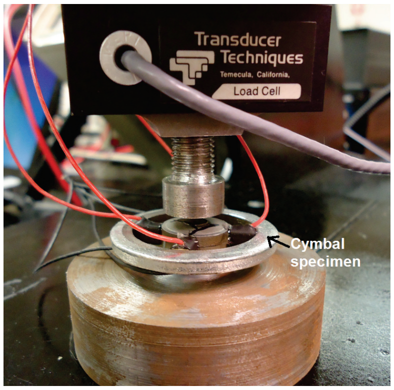

Figure 14: Photograph of Closed-up Cymbal Specimen in the Test Rig.

B. Test Results

Figs. 15, 16 and 17 show measured cyclic load and corresponding open-circuit output voltage for 800 N, 1,500 N, and 2,100 N respectively. The cymbal specimen was tested with two configurations in parallel and in series. The results in the figures were for in series.

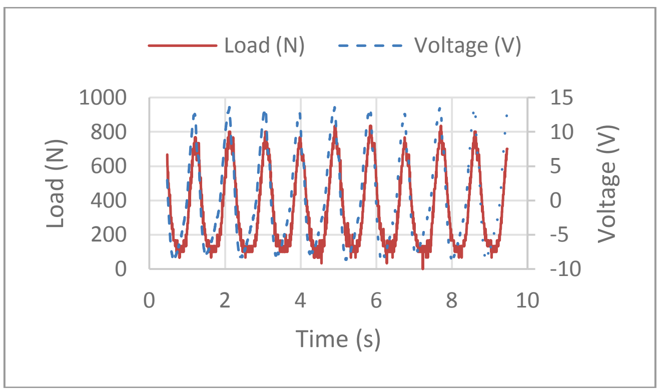

Figure 15: Measured Cyclic Load and Open-circuit Output Voltage for 800 N.

Measured cyclic loads also indicate that performance of the cost-effective test rig is acceptable.

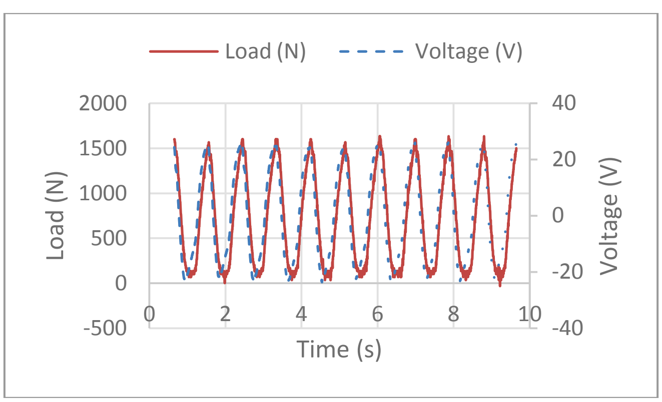

Figure 16: Measured Cyclic Load and Open-circuit Output Voltage for 1,500 N.

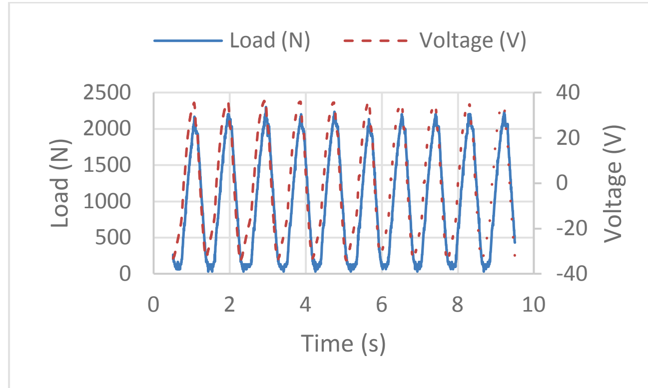

Figure 17: Measured Cyclic Load and Open-circuit Output Voltage for 2,100 N.

The currents were also measured for each load. The measured currents were 2.9 μA, 6.8 μA, and 9.7 μA for 800 N, 1,500 N, and 2,100 N, respectively. The comparison of measured open-circuit voltages in series for three different cyclic loads is shown in Table 1.

Table 1: Comparison of Open-circuit Output Voltages in Series for Different Cyclic Loads.

Load (N)	Measured output voltage (V)
800	10.58 ± 2.67
1500	23.9 ± 1.38
2100	34.50 ± 1.33
$\pm$: sample standard deviation from nineteen peaks	

Comparing to the result from unimorph cymbal design [3], this restructured cymbal generates higher energy in parallel. In addition, this design may be much more advantageous for longevity performance because of no bonging layer. The bonding layer of the unimorph cymbal design was influenced by extremely high shear load, which is not desirable.

IV. CONCLUSION

New low-profile cymbal energy harvesters using a piezoelectric ring transducer and set of PZT stacks are designed and tested in this paper. The restructured cymbal harvester with four set of PZT stacks generates higher energy in parallel than that of unimorph cymbal design. It may also provide better longevity performance because there is no bonding layer. Longevity test will be carried out in near future. In addition, comprehensive analysis to predict generating energy and parametric study for performance optimization is currently conducting.

REFERENCES

[1] D. Arnold, W. Kinsel, W. Clark, and C. Mo, "Exploration of New Cymbal Design in Energy Harvesting," *Proc. of SPIE, Smart Structures and Materials*, Mar. 6-10, San Diego, CA, 2011.

[2] C. Mo, D. Arnold, W. Kinsel, and W. Clark, "Unimorph PZT Cymbal Design in Energy Harvesting," *ASME Conf. on Smart Materials Adaptive Structures and Intelligent Systems*, Sept. 18-21, Scottsdale, AZ., 2011.

[3] C. Mo, D. Arnold, W. Kinsel, and W. Clark, "Modeling and Experimental Validation of Unimorph PZT Cymbal Design in Energy Harvesting," *Journal of Intelligent Material Systems and Structures*, Vol. 24(7), pp. 828-836, 2013.

[4] C. Mo, S. Jordan, and W. Clark, "Bimorph Piezoelectric Cymbal Design in Energy Harvesting," *ASME Conf. on Smart Materials, Adaptive Structures and Intelligent Systems*, Stone Mountain, GA, 19-21 September, 2012.

[5] H. Kim, A. Bartra, S. Priya, K. Uchino, and D. Markley, "Energy Harvesting Using a Piezoelectric Cymbal Transducer in Dynamic Environment," *Japanese Journal of Applied Physics*, Vol. 43(9A), pp. 6178-6183, 2004.

[6] H. Kim, S. Priya, K. Uchino, and R. Newham, "Piezoelectric Energy Harvesting under High Pre-Stressed Cyclic Vibrations," *Journal of Electroceramics,* Vol. 15, pp. 27-34, 2005.

[7] H. Kim, S. Priya, and K. Uchino, "Modeling of Piezoelectric Energy Harvesting Using Cymbal Transducers," *Japanese Journal of Applied Physics*, Vol. 45(7), pp. 5836-5840, 2006.

[8] J. Yuan, X. Shan, T. Xie, and W. Chen, "Modeling and Improvement of a Cymbal Transducer in Energy Harvesting," *Journal of Intelligent Material Systems and Structures*, Vol. 21(8), pp. 765-771, 2010.

[9] S. Platt, S. Farritor, K. Garvin, and H. Haider, "The Use of Piezoelectric Ceramics for Electric Power Generation Within Orthopedic Implants," *IEEE/ASME Trans on Mechatronics*, Vol. 10(4), pp. 455-461, 2005.

[10] S. Platt, S. Farritor, and H. Haider, "On Low-Frequency Electric Power Generation With PZT Ceramics," *IEEE/ASME Trans on Mechatronics*, Vol. 10(2), pp. 240-252, 2005.

[11] H. Chen, C. Jia, C. Zhang, Z. Wang, and C. Liu, "Power Harvesting With PZT Ceramics," *IEEE International Symposium on Circuits and Systems*, 27-30 May, New Orleans, LA., pp. 557-560, 2007.

[12] D. D'Lima, S. Patil, N. Steklov, J. Slamin, and C. Colwell, "Tibial Forces Measured In Vivo after Total Knee Arthroplasty," *The Journal of Arthroplasty*, Vol. 21(2), pp. 255-262, 2006.

[13] B. Kirking, J. Krevolin, C. Townsend, C. Colwell, and D. D'Lima, "A multiaxial force-sensing implantable tibial prosthesis," *Journal of Biomechanics*, Vol. 39, pp. 1744-1751, 2006.

[14] S. Sivarasu and M. Lazar, "Finite Element Analysis of a Novel High Flexion Knee (Ti-UHMWPE) used in Total Knee Arthroplasty," *The Internet Journal of Bioengineering*, Vol. 4(1), 2009.

[15] A. Ugural, *Stresses in Plates and Shells*, 2nd edition, Boston, McGraw-Hill, Inc, 1999.

[16] W. Young, *Roark's Formulas for Stress & Strain*, McGraw-Hill, Inc, New York, 6th Ed., 1989.

[17] IEEE Standard 176, *IEEE Standards on Piezoelectricity*, The Institute of Electrical and Electronics Engineers, 1978.